Inorganica Chimica Acta 477 (2018) 24–30

Contents lists available at ScienceDirect

Inorganica Chimica Acta

journal homepage: www.elsevier.com/locate/ica

Research paper

Can pendant pyridyl arm assist the proton delivery in electrocatalysis?

Siyuan Luo [a], Didjay F. Bruggeman [a], Maxime A. Siegler [b], Elisabeth Bouwman [a,*]

[a] Leiden Institute of Chemistry, Gorlaeus Laboratories, Leiden University, P.O. Box 9502, 2300 RA Leiden, The Netherlands
[b] Department of Chemistry, Johns Hopkins University, 3400 N. Charles Street, Baltimore, MD 21218, USA

ARTICLE INFO

Article history:
Received 10 October 2017
Received in revised form 20 February 2018
Accepted 21 February 2018
Available online 22 February 2018

ABSTRACT

Two nickel(II) complexes [Ni(**L1**)$_2$]Br$_2$ and [Ni(**L2**)$_2$]Br$_2$ (H**L1**Cl = 1-benzyl-3-(pyridin-2-ylmethyl)benzimidazolium chloride; H**L2**Cl = 1,3-bis(pyridin-2-ylmethyl)benzimidazolium chloride) were synthesized as non-noble metal catalysts for the electrocatalytic hydrogen evolution reaction. Single crystal X-ray crystallography revealed that the nickel metal centers in both compounds are in a square-planar geometry with like donor atoms of the two bidentate ligands in *cis* positions. The redox properties of the two compounds were studied using cyclic voltammetry. Electrocatalytic proton reduction experiments using these complexes were performed in DMF with acetic acid as the proton source. Compound [Ni(**L2**)$_2$]Br$_2$, containing two free pyridyl groups, not only exhibits higher electrocatalytic activity, but also has a smaller overpotential for the reduction of protons. The comparison of these results provides convincing experimental evidence for the pyridyl group acting as proton relay during the proton reduction process, although unfortunately the performance of the compounds is rather low.
© 2018 The Authors. Published by Elsevier B.V. This is an open access article under the CC BY license (http://creativecommons.org/licenses/by/4.0/).

1. Introduction

Ligands with pendant, non-coordinating Lewis bases have received ample attention from inorganic chemists, because the additional Lewis base might affect the performance of molecular catalysts by providing binding sites for protons [1–4]. Notably, the introduction of base-functionalized pendant arms in the ligands of molecular catalysts has been quite important in the electrochemical research area for assisting in proton-coupled electron-transfer processes [5–8]. For example, Ni-diphosphane complexes bearing pendant amines as proton-binding sites have been shown to exhibit extremely high activity (TOF > 100,000 s^{-1}) in electrocatalytic H_2 evolution [9]. The molecular design of catalysts using pendant Lewis bases is inspired by the structures of natural enzymes, in which nearby amino acids close to the active site play are involved in temporary proton storage [8–11]. With the aim to investigate the role of the pendant amine group in dihydrogen evolution, DuBois' group compared the electrocatalytic activity of the compound [Co($P^{Ph}_2N^{Ph}_2$)(CH_3CN)$_3$](BF_4)$_2$ ($P^{Ph}_2N^{Ph}_2$ = 1,3,5,7-tetraphenyl-1,5-diaza-3,7-diphosphacyclooctane) incorporating pendant amines, with that of the compound [Co(dppp)(CH_3CN)$_3$](BF_4)$_2$ (dppp = 1,3-bis(diphenylphosphanyl)propane) without pendant amines [10]. Although the two cobalt compounds are equipped with similar diphosphane ligands, the investigations showed that only the former one possesses catalytic activity in proton reduction.

Not only secondary or tertiary amines but also the pyridyl group can realize the function as a proton relay [7,12–14]. Recent DFT calculations on a pyridyl-functionalized cobalt diimine-dioxime catalyst have indicated that the non-coordinated pyridyl pendant group may help to reduce the energetic barrier for hydride formation in electrolysis [7]. Indeed it has been suggested that the pyridyl group may facilitate the reaction of a metal-hydride intermediate with a nearby proton [14]. In the research described in this paper, we aimed to explore the role of uncoordinated pyridyl groups in the proton reduction activity of nickel compounds with carbene ligands.

In the design of metal-carbene complexes pyridine-functionalized (benz)imidazole-2-ylidene ligands have received a lot of attention. Coordination compounds of these functionalized carbenes have been reported for a large array of metal centers such as Ag, Hg, Pd, Au, Ni, Ru and Pt [15–20]. For one and the same ligand, the configuration of the complexes will largely depend on the properties of the metal center. Setting the ligand precursor 1,3-bis(pyridin-2-ylmethyl)benzimidazolium chloride H**L2**Cl as an example, Pt^{II} and Pd^{II} ions can coordinate with one ligand in a tridentate mode with both pyridines bound in square-planar geometries [15,20]; Ru^{II} ions may bind two ligands in a tridentate mode in an octahedral geometry [20], whereas Ag^{I} and Au^{I} ions can bind either one [17] or two ligands [19] with both pyridine arms non-coordinated.

* Corresponding author.
E-mail address: bouwman@chem.leidenuniv.nl (E. Bouwman).

https://doi.org/10.1016/j.ica.2018.02.030
0020-1693/© 2018 The Authors. Published by Elsevier B.V.
This is an open access article under the CC BY license (http://creativecommons.org/licenses/by/4.0/).

Herein, we report the synthesis and characterization of two new nickel complexes of pyridyl-functionalized carbene ligands based on benzimidazole and the study of their electrocatalytic activity in H_2 evolution. We sought to determine whether the presence of pendant pyridyl groups could enhance H_2 evolution by acting as an intramolecular proton shuttle in electrocatalysis by comparing these two related compounds. *N*-heterocyclic carbenes are widely recognized as innocent ligands in organometallic chemistry [21]. The influence of a pendant pyridine arm in electrocatalysis might be more readily understood in the absence of other redox-active functional groups.

2. Result and discussion

2.1. Synthesis of the complexes

The ligand precursors 1-benzyl-3-(pyridin-2-ylmethyl)benzimidazolium chloride (H**L1**Cl) [22] and 1,3-bis(pyridin-2-ylmethyl) benzimidazolium chloride (H**L2**Cl) [20] were synthesized following literature methods with small modifications, in good yields of 77% and 87%, respectively. The nickel(II) bromide compounds [Ni(**L1**)$_2$]Br_2 and [Ni(**L2**)$_2$]Br_2 were obtained as yellow-colored powders from a melt of nickel acetate with these ligand precursors in tetrabutylammonium bromide (TBAB) in vacuum (Scheme 1). The complexes were characterized by NMR spectroscopy and electrospray ionization mass spectrometry (ESI-MS). The successful creation of the carbene moieties and their coordination to the nickel(II) center is indicated by the absence in the ^{1}H NMR spectra of the characteristic downfield signals for the imidazolium NCHN protons (10–10.5 ppm) in both complexes. The sharp and clear ^{1}H NMR spectrum of [Ni(**L1**)$_2$]Br_2 is in agreement with a low-spin square-planar nickel ion. In contrast, in the ^{1}H NMR spectrum of [Ni(**L2**)$_2$]Br_2 the peaks are rather broad (see next section and Fig. S1). This broadening most likely is caused by a binding and dissociation equilibrium of the pyridyl groups in the nickel compound [Ni(L2)$_2$]Br_2, in solution resulting in a mixture of the low-spin square-planar nickel complex with 5-coordinate or octahedral species containing high-spin nickel centers. As can be seen from the NMR spectrum in Fig. S1, this must comprise only a very small part of the nickel ions, as the NMR peaks are all in the diamagnetic region, but just are slightly broadened. The ESI-MS spectra exhibit base peaks corresponding to the $[M-2Br]^{2+}$ cationic complexes. Crystalline samples of the Ni compounds were dried in vacuo before elemental analysis was performed; however, the analytical results indicate that the water molecules found in the crystal lattice were not totally removed. During synthesis of the complexes the chloride counter ions of the ligands were replaced by the bromide ion from TBAB.

2.2. Structural characterization of the complexes

Single crystals of [Ni(**L1**)$_2$]Br_2 and [Ni(**L2**)$_2$]Br_2 suitable for X-ray structure determination were obtained using the liquid-liquid diffusion method. The crystallographic and refinement data are collected in Table S1. Projections of the structures of the cationic nickel centers in [Ni(**L1**)$_2$]Br_2 and [Ni(**L2**)$_2$]Br_2 are shown in Fig. 1. Selected bond distances and angles are provided in Table 1.

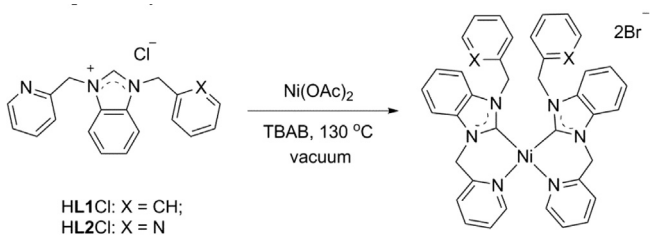

Scheme 1. Synthesis route of the compounds [Ni(**L1**)$_2$]Br_2 and [Ni(**L2**)$_2$]Br_2.

The compound [Ni(**L1**)$_2$]Br_2 crystallizes in the space group *P-1*, whereas the compound [Ni(**L2**)$_2$]Br_2 crystallizes in the monoclinic space group *Cc*. Both compounds crystallized with two independent cationic complexes, four bromide ions and some disordered solvent molecules in the asymmetric unit. The coordination environment of the nickel centers in the two independent molecules is very similar, and for both compounds, the relevant bond distances and angles from only one of the two molecules are provided. The nickel ion in $[Ni(\mathbf{L1})_2]^{2+}$ is found in a four-coordinate square planar geometry in which two ligands are bound in a bidentate C, N fashion with the C and N donor atoms in mutual *cis* positions (Fig. 1a). Although the ligand **L2** potentially is a tridentate ligand, in $[Ni(\mathbf{L2})_2]^{2+}$ the nickel ion is also found in a square-planar geometry with donor atoms of the two bidentate ligands in *cis* positions (see Fig. 1b).

The Ni—C bond distances in the two compounds are around *ca.* 1.87 Å whereas the Ni—N bonds are *ca.* 1.94 Å. Both the Ni—C and Ni—N bond distances are shorter by 0.2 Å in comparison with the reported Ru [20], Pd [15,16], and Au compounds [19], which can be attributed to the smaller ionic radius of the nickel ion. In the compound [Ni(**L2**)$_2$]Br_2 the nitrogen atom of one of the pendant pyridyl groups resides in an apical position of the nickel center at a distance of *ca.* 2.98 Å; if this interaction is taken into account the geometry of the nickel ion may be regarded as a distorted square pyramid (Fig. 1c). This additional weak interaction of the pyridyl group may be retained in solution, or even be stronger, thus causing the rather broad signals observed in the ^{1}H NMR spectra of this compound.

The square-planar geometries of the nickel ions in [Ni(**L1**)$_2$]Br_2 and [Ni(**L2**)$_2$]Br_2 were evaluated with an equation derived from a report by Yang [23,24]. The largest and second-largest L—Ni—L angles in [Ni(**L1**)$_2$]Br_2 are 171.7(1)° and 174.0(1)°, resulting in a τ_4 value of 0.100 indicative of only a very slight distortion of the square-planar geometry. For compound [Ni(**L2**)$_2$]Br_2 a τ_4 value of 0.023 is calculated, indicating that the geometry of the central ion (not taking into account the axial coordination of pyridine) is close to the ideal square-planar geometry.

Complexes of other metal ions bearing the ligand **L2** have been reported by Adhikary et al. [20]. Pt(II) was found to coordinate with one ligand **L2** to form the complex [Pt(**L2**)Cl]PF_6 with the Pt(II) ion in a square-planar geometry, whereas the Ru(II) ion binds two ligands **L2** to form the compound [Ru(**L2**)$_2$]$(PF_6)_2$ with the ruthenium center in an octahedral geometry. A structure has been reported of a nickel compound containing two 1,3-bis(pyridin-2-ylmethyl)imidazolium ligands, in which similar to [Ni(**L2**)$_2$]Br_2 the ligands are arranged with like donor atoms in *cis* positions [16]. The nickel ion in this compound is also in a square-planar geometry and one of the pendant pyridyl groups resides in an apical position of the nickel center at a distance of 3.345 Å, significantly larger than the one in [Ni(**L2**)$_2$]Br_2.

2.3. Electrochemical properties of the complexes

The redox potentials of the nickel compounds were evaluated using cyclic voltammetry. The electrochemical potentials all are reported relative to the Ag/AgCl reference electrode. The cyclic voltammogram (CV) of [Ni(**L1**)$_2$]Br_2 shows two reductive waves, the first of which is reversible at a scan rate of 0.1 V/s (Fig. 2). The reversible redox process located at $E_{1/2} = -1.00$ V vs. Ag/AgCl is diffusion controlled, as shown by the linear dependence of the peak current on the square root of the scan rate (Fig. S2). This redox wave is characterized by a peak-to-peak separation ΔE_p of 80 mV

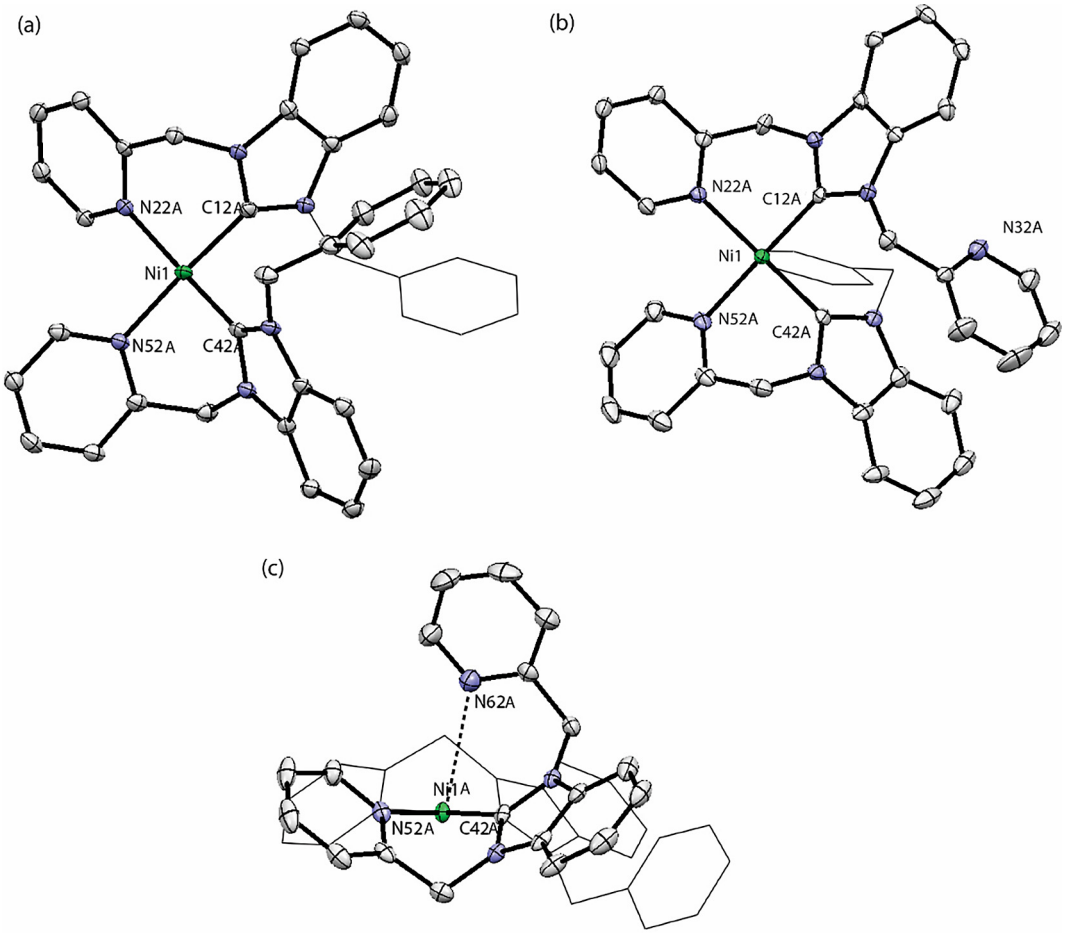

Fig. 1. Displacement ellipsoid plots of the cationic complexes (a) $[Ni(\mathbf{L1})_2]Br_2$, (b) and (c) $[Ni(\mathbf{L2})_2]Br_2$ are drawn at 50% probability level with selected atom numbering. For clarity the hydrogen atoms, bromide ions, solvent molecules and the lattice water molecules are omitted and parts of the ligands are displayed in wireframe.

Table 1
Selected bond distances (Å) and angles (°) of the compounds $[Ni(\mathbf{L1})_2]Br_2$ and $[Ni(\mathbf{L2})_2]Br_2$.

	$[Ni(\mathbf{L1})_2]Br_2$	$[Ni(\mathbf{L2})_2]Br_2$
Ni1–C12A	1.880(3)	1.860(4)
Ni1–C42A	1.872(2)	1.863(4)
Ni1–N22A	1.947(2)	1.938(4)
Ni1–N52A	1.953(2)	1.950(4)
Ni1…N62A	–	2.984(4)
N52A–Ni1–N22A	95.10(9)	91.25(15)
N52A–Ni1–C42A	86.47(10)	87.32(17)
C42A–Ni1–C12A	93.12(11)	94.33(18)
C12A–Ni1–N22A	86.15(10)	87.09(17)
N52A–Ni1–C12A	174.00(10)	178.08(18)
C42A–Ni1–N22A	171.71(11)	178.56(17)

(in our conditions ΔE_p for the $Fc^{0/+}$couple was found to be 95 mV), indicating a one-electron transfer. Thus, we assign this first wave to a Ni(II)/Ni(I) redox process. The quasi-reversible reduction event at −1.29 V is tentatively ascribed to a Ni(I)/Ni(0) redox process. The assignment of these two redox waves to nickel-centered reductions is supported by the fact that the ligand precursor H**L1**Cl is electrochemically inert in the range of 0 to −1.5 V. The second reductive wave at −1.29 V gradually becomes reversible with increasing scan rate, whereas the wave becomes less reversible with decreasing scan rates (see Fig. S3). This behavior indicates the occurrence of a dissociative electron transfer (DET) process [25], meaning that after the reduction of $[Ni^{II}(\mathbf{L1})_2]^{2+}$ to $[Ni^{I}(\mathbf{L1})_2]^{+}$

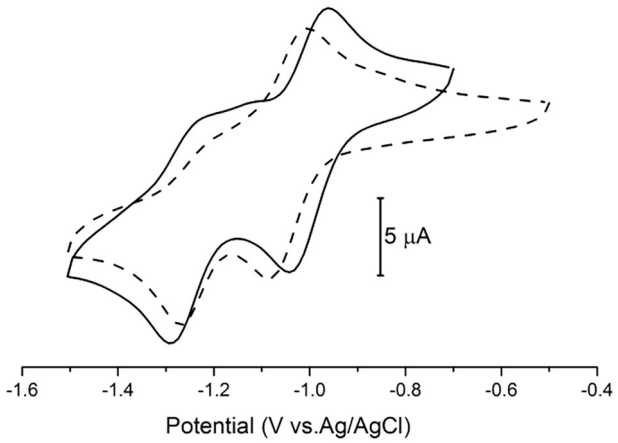

Fig. 2. CVs of the compounds $[Ni(\mathbf{L1})_2]Br_2$ (solid line) and $[Ni(\mathbf{L2})_2]Br_2$ (dashed line). Experiments were performed at a complex concentration of 1 mM in DMF with 100 mM $TBAPF_6$ as the supporting electrolyte at scan rate 0.1 V/s, using a glassy carbon working electrode.

a stepwise chemical reaction is coupled to the second electron transfer, generating a new product.

Similarly, the CV of compound $[Ni(\mathbf{L2})_2]Br_2$, containing two uncoordinated pyridyl groups, shows one reversible redox process at $E_{1/2}$ = −1.05 V followed by an irreversible reductive process at −1.27 V (Fig. 2). The first reversible redox process of $[Ni(\mathbf{L2})_2]Br_2$

is at a slightly more negative potential than that of [Ni(**L1**)$_2$]Br$_2$, indicating a slightly higher electron density at the nickel center, likely because of the interaction with one or both of the pendant pyridyl groups in solution. The reversibility of the second reductive wave at E_{pc2} = −1.29 V of this tetrapyridyl-functionalized compound [Ni(**L2**)$_2$]Br$_2$ appeared not to depend on the scan rate. Even when the scan rate was increased to 500 mV/s the second reductive process still was quasi-reversible (see Fig. S4). The electrochemical data are summarized in Table 2.

2.4. Electrocatalytic activity for proton reduction in DMF

The two compounds were examined for their activity in the electrocatalytic proton reduction in DMF, using acetic acid (HOAc) as a weak proton source. Before each scan the working electrode was freshly polished.

Compared to the CV of acetic acid (10 mM) in DMF, after addition of either the complex [Ni(**L1**)$_2$]Br$_2$ or [Ni(**L2**)$_2$]Br$_2$ a relatively large current indicating the reduction of protons was observed at a potential around −2 V vs Ag/AgCl (Fig. 3). Two small irreversible peaks appear before the electrocatalytic wave, approximately at −1.04 V and −1.17 V for [Ni(**L1**)$_2$]Br$_2$ and at −1.09 V and −1.20 V for [Ni(**L2**)$_2$]Br$_2$. These peaks were broad and close to each other making it difficult to identify them separately. Only a broad plateau can be recognized when showing these waves together with the following catalytic wave. A zoom of CVs (ranging from −0.5 V to −1.5 V) is provided in Fig. S5.

For both compounds the first small reductive wave occurs at the exact same potential where the metal-centered Ni^{II}/Ni^{I} reduction process was observed (see previous section and Fig. S5). The second small reductive potential occurs at a more positive potential compared to the ones in the absence of acid, indicating that there is a chemical step before the second electron transfer takes place. The electrocatalysis therefore most likely proceeds via an ECEC mechanism [26]. The catalytic onset potential for proton reduction in presence of [Ni(**L2**)$_2$]Br$_2$ (at −1.6 V) occurs at a lower potential than in the presence of [Ni(**L1**)$_2$]Br$_2$ (at −1.8 V). Furthermore, in the same conditions the compound [Ni(**L2**)$_2$]Br$_2$ shows the larger catalytic current, indicating a higher electrocatalytic activity than that of [Ni(**L1**)$_2$]Br$_2$ (Fig. 3).

With the aim to compare the electrocatalytic activity of the two compounds in a more quantitative way, controlled-potential coulometry experiments (CPC) were carried out. The charge consumptions over time of solutions containing just the pure acid or each of the catalysts were also recorded separately as references. The charge accumulation graphs show that over a period of 10 min charge consumption is negligible for the solutions containing only acid or only the nickel compounds (Fig. 4). However, continuous charge consumption was recorded for solutions containing both acid and one of the nickel catalysts. The quantity of dihydrogen gas generated during the CPC experiments can be estimated from the charge consumption of solutions containing both the nickel compound and the acid, after subtraction of the charge consumption of the blanks. The two complexes [Ni(**L1**)$_2$]Br$_2$ or [Ni(**L2**)$_2$]Br$_2$ are estimated to produce 3×10^{-4} mmol and 5×10^{-4} mmol H_2 respectively in 10 min in presence of 6×10^{-3} mmol catalyst at a potential of −1.80 V (assuming that all electrons are used in proton reduction). Almost a doubled charge consumption was found for the complex [Ni(**L2**)$_2$]Br$_2$ equipped with two additional pendant pyridine groups, indicating a higher catalytic activity. However, despite this improvement, still the electrocatalytic activity of [Ni(**L2**)$_2$]Br$_2$ is disappointingly low.

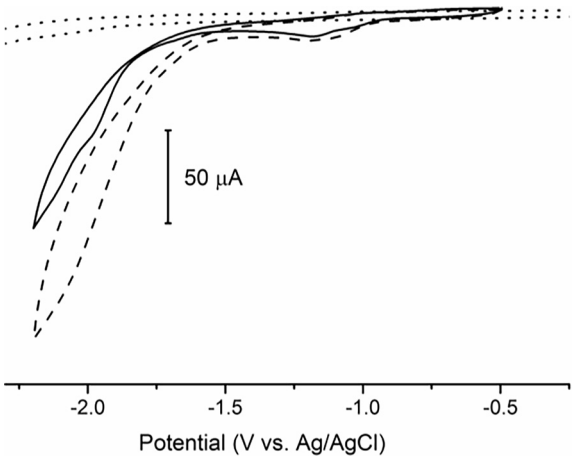

Fig. 3. CVs of 10 mM acetic acid in presence of 1 mM complex [Ni(**L1**)$_2$]Br$_2$ (solid line), in the presence of 1 mM complex [Ni(**L2**)$_2$]Br$_2$ (dashed line) and in the absence of a complex (dotted line) in DMF containing 0.1 M $TBAPF_6$ as supporting electrolyte at scan rate 0.1 V/s, using a glassy carbon working electrode.

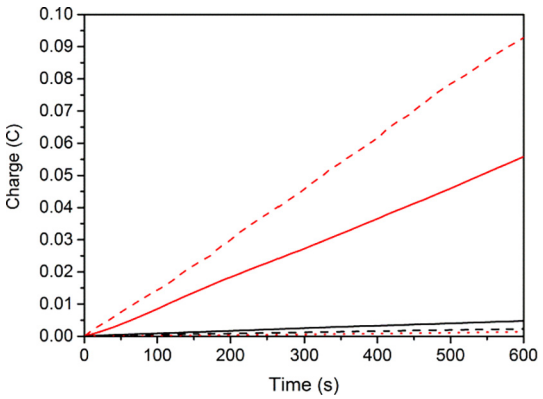

Fig. 4. Charge vs. time plot over 600 s during CPC at potential of −1.8 V. Black lines: compounds in absence of acid; Red lines: compounds in presence of 50 mM acetic acid (solid = [Ni(**L1**)$_2$]Br$_2$, dashed = [Ni(**L2**)$_2$]Br$_2$); Dotted red line: 50 mM acetic acid only. (For interpretation of the references to colour in this figure legend, the reader is referred to the web version of this article.)

Generally, the mechanism can be divided in three steps for a hydrogen-evolution process based on a metal-containing homogenous catalyst. The first step is the reduction of the metal center; if the metal center is equipped with an electron-withdrawing ligand, the metal center is more readily reduced. The second step is the formation of the metal hydride intermediate, which is facilitated by the presence of an electron-donating ligand. The third step is the generation of dihydrogen: the metal-hydride intermediate

Table 2
Electrochemical data of the nickel compounds.[a]

	E_{pc1} [V]	E_{pa1} [V]	$E_{1/2}$ [V] (ΔE_p [mV])	E_{pc2}[V]
[Ni(**L1**)$_2$]Br$_2$	−1.04	−0.96	−1.00 (80)	−1.29
[Ni(**L2**)$_2$]Br$_2$	−1.09	−1.01	−1.05 (80)	−1.27

[a] Potentials are given vs. the Ag/AgCl electrode. All voltammograms were recorded in DMF. Conditions: scan rate = 0.1 V/s, compound (1 mM), $TBAPF_6$ (0.1 M), using glassy-carbon working electrode.

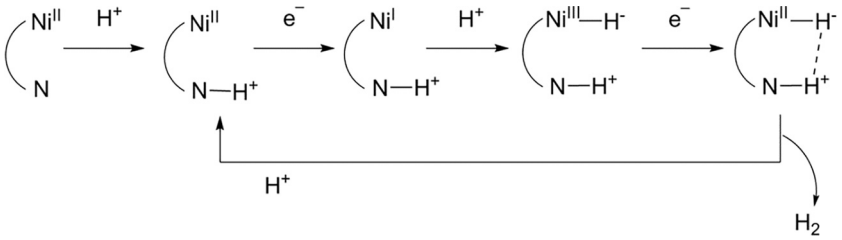

Scheme 2. Proposed mechanism of the electrocatalytic reduction of protons by [Ni(**L2**)$_2$]Br$_2$.

reacts with another proton and electron to release dihydrogen [27]. Based on this mechanism, generally a molecular catalyst will work at a small overpotential but with relatively low efficiency for electron-withdrawing ligands, or with high efficiency but at relatively larger overpotentials for electron-donating ligands.

As discussed in the previous section, the ligand **L2** is the more electron donating of the two in absence of acid, so that the nickel center in [Ni(**L2**)$_2$]Br$_2$ is reduced at more negative potentials. Unexpectedly, the compound [Ni(**L2**)$_2$]Br$_2$ not only shows higher electrocatalytic activity but also a smaller overpotential (Fig. 3). Thus, the presence of the free pyridyl pendant arms in the compound [Ni(**L2**)$_2$]Br$_2$ apparently reduces the overpotential for the electrocatalytic proton reduction. The additional pyridine groups act as an intramolecular proton acceptor and proton shuttle assisting in the generation of dihydrogen [7]. Based on the assistance of the pyridyl groups for complex [Ni(**L2**)$_2$]Br$_2$ the catalytic mechanism tentatively can be described as shown in Scheme 2. First the non-coordinated pyridyl groups are protonated in the presence of acid. Then the metal center is reduced to Ni^{I}, followed by the formation of a metal-hydride. Finally the hydride reacts with the proton on the pyridyl arm with the release of dihydrogen.

3. Conclusion

Two nickel(II) complexes [Ni(**L1**)$_2$]Br$_2$ and [Ni(**L2**)$_2$]Br$_2$ with different ligands were synthesized as non-noble metal molecular catalysts for the hydrogen evolution reaction. The nickel center in both compounds is in a square-planar geometry with two bidentate ligands in *cis* arrangements. The binding of two potentially tridentate ligands in this configuration in the structure of [Ni(**L2**)$_2$]Br$_2$ results in the presence of two free pyridine groups. The redox properties of the two complexes were determined using cyclic voltammetry and the electrocatalytic dihydrogen generation with these complexes in DMF was studied using acetic acid as the proton source. The complex [Ni(**L2**)$_2$]Br$_2$ containing two free pyridyl groups exhibited not only the higher activity in electrocatalysis, but also a smaller overpotential for proton reduction. This result indicates that the presence of the free pyridyl groups help to break the anti-correlation between the energy of the reduction and the catalytic activity. The comparison of the catalytic properties of these two related structures (both with redox-innocent carbene backbones) provide convincing experimental evidence of the pyridyl group acting as proton relay during the proton reduction process. Unfortunately, it appears that this type of carbene-based ligands in combination with nickel do not yield very active electrocatalysts for proton reduction.

4. Experimental

4.1. Materials

Commercial chemicals were used without further purification. Acetonitrile and diethyl ether were obtained from a PureSolv MD5 solvent dispenser. Dry methanol and dimethylformamide were prepared by adding molecular sieves into commercial anhydrous solvent. All air-sensitive reactions were performed under argon or dinitrogen gas using standard Schlenk techniques unless mentioned otherwise.

4.2. Analytical methods

^{1}H and ^{13}C spectra were recorded on a Bruker 300 DPX/Bruker 400 AV spectrometer. Mass spectra were obtained using a Finnigan Aqua Mass Spectrometer (MS) with electrospray ionization (ESI). Elemental analyses were performed by the Mikroanalytisches Laboratorium Kolbe, Germany.

Cyclic voltammetry was recorded with an Autolab PGstat10 potentiostat controlled by GPES4 software under argon. A 3 mm diameter glassy carbon electrode was used as working electrode and a Pt wire as the counter electrode. The experimental reference was an Ag/AgCl electrode in the electrolyte solution. Cyclic voltammety was performed in dry DMF with 0.1 M tetrabutylammonium hexafluoridophosphate ($TBAPF_6$) as the supporting electrolyte under a stream of argon at room temperature. All potentials are given versus Ag/AgCl. Ferrocene was added after each experiment as an internal standard. Under these conditions the $Fc^{0/+}$ couple was located at $E_{1/2}$ = 0.510 V vs. Ag/AgCl with a ΔE_p of 95 mV. The working electrode surface was polished, ultrasonically cleaned and rinsed before each single CV measurement.

Controlled-potential coulometry (CPC) experiments were carried out with an Autolab PGstat10 potentiostat controlled by GPES4 software under argon. A 3 mm diameter glassy carbon electrode was used as working electrode and a platinum wire as the counter electrode. 1 mM complex and 50 mM acetic acid were added in 6 mL dry degassed DMF with 0.1 M $TBAPF_6$ as the supporting electrolyte under a stream of argon at room temperature. A CPC experiment was run at −1.8 V for 600 s, while the solution was stirred continuously. The blank and reference CPC experiments (only acid or only catalyst added) were performed using the same conditions.

4.3. Single crystal X-ray crystallography

All reflection intensities were measured at 110(2) K using a SuperNova diffractometer (equipped with Atlas detector) with Mo $K\alpha$ radiation (λ = 0.71073 Å) under the program CrysAlisPro (Version 1.171.36.32 Agilent Technologies, 2013). The same program was used to refine the cell dimensions and for data reduction. The structure was solved with the program SHELXS-2014/7 [28,29], and was refined on F^2 with SHELXL-2014 [28,29]. Numerical absorption correction based on gaussian integration or analytical numeric absorption correction over a multifaceted crystal model was applied using CrysAlisPro. The temperature of the data collection was controlled using the system Cryojet (manufactured by Oxford Instruments). The H atoms were placed at calculated positions (unless otherwise specified) using the instructions AFIX 23 or AFIX 43 with isotropic displacement parameters having val-

ues 1.2 or 1.5 *U*eq of the attached C atoms. For [Ni(**L1**)$_2$]Br$_2$, the H atoms attached to O1W (ordered lattice water molecule) and O2W (only for the major component of the disorder) could be retrieved from difference Fourier maps. Their coordinates were refined freely but the O—H and H…H distances were restrained to be 0.84(1) and 1.33(1) Å, respectively. For [Ni(**L2**)$_2$]Br$_2$, the O—H and H…H distances were restrained to be 0.84(3) and 1.33(3) using the DFIX instruction. The atoms attached to O4W, O5W, O6W, O7W, O8W and O9W (partially occupied or disordered lattice water molecules) could not be retrieved.

The structure of [Ni(**L1**)$_2$]Br$_2$ is partly disordered. One phenyl group (C61A-C66A) and one Br$^-$ counter ion are found disordered over two orientations; the occupancy factors of the major components of the disorder refine to 0.59(4) and 0.923(5), respectively. One of the three lattice water molecule (O2W) is disordered over three orientations, and the occupancy factors refine to 0.808(3), 0.109(3) and 0.083(3). The occupancy of the lattice water molecule O3W was refined freely, and its value refines to 0.639(8). The H atoms attached to O3W could not be retrieved. ADDSYM detects a pseudo translation of ½ **a** + ½ **c**. However, the conformations of the two crystallographically independent molecules are different as the orientations of the phenyl groups are significantly different.

The structure of [Ni(**L2**)$_2$]Br$_2$ is partly disordered. One of the pyridine rings (from molecule A) is found to be disordered over two orientations, and the occupancy factor of the major component of the disorder refines to 0.52(2). In the asymmetric unit, there are five Br$^-$ sites with all occupancies lower than 1. Two sites (Br1 and Br2) are ordered, and their occupancy factors refine to 0.940(2) and 0.942(2), respectively. The remaining counter ions (Br3/Br3′, Br4/Br4′ and Br5/Br5′) are disordered over two orientations. The occupancies factors for Br3, Br3, Br4, Br4′, Br5 and Br5′ refine to 0.853(3), 0.086(3), 0.624(2), 0.0494(15), 0.391(2) and 0.1149(16), respectively. The sum of all occupancies factors for the Br$^-$ counter ions was restrained to be 4 using the SUMP instruction. The occupancy factors for O4W/O4W' (disordered), O5W/O5W' (disordered), O6W, O7W, O8W and O9W refine to 0.434(11)/0.566(11), 0.715(8)/0.285(8), 0.674(15), 0.671(16), 0.429(18) and 0.41(2), respectively.

CCDC-1511049 and 1,511,050 for [Ni(**L1**)$_2$]Br$_2$ and [Ni(**L2**)$_2$]Br$_2$ contain the supplementary crystallographic data for this paper. These data can be obtained free of charge from The Cambridge Crystallographic Data Center via www.ccdc.cam.ac.uk/data_request/cif.

4.4. Ligand and complex synthesis

N-Pyridylmethyl-benzimidazole, [30] ligand precursors H**L1**Cl [22], H**L2**Cl [20], and the complexes [Ni(**L1**)$_2$]Br$_2$ and [Ni(**L2**)$_2$]Br$_2$ [31–33] were synthesized following literature methods with small modifications.

4.5. [Ni(*L1*)$_2$]Br$_2$

H**L1**Cl (0.67 g, 2 mmol), anhydrous Ni(OAc)$_2$ (0.17 g, 1 mmol) and tetrabutylammonium bromide (1.5 g) were weighed into a 10 mL round-bottomed flask and dried for 4 h at 80 °C in a Schlenk setup under vacuum. The reaction mixture was stirred for 48 h at 130 °C under vacuum. The mixture was then cooled to room temperature and triturated with H_2O. The water layer was washed with DCM (3 × 20 mL) and evaporated to dryness. The remaining solid was dissolved in a mixture of acetonitrile and methanol and a yellow crystalline solid was obtained using liquid to liquid diffusion method with diethyl ether in 12% yield (90 mg). ^{1}H NMR (400 MHz, DMSO-d_6) δ 8.26–8.13 (m, 4H), 8.12–7.99 (m, 4H), 7.48 (q, *J* = 8.0, 7.1 Hz, 4H), 7.32 (dt, *J* = 15.3, 8.0 Hz, 4H), 7.10–6.94 (m, 10*H*), 6.82 (d, *J* = 15.5 Hz, 2H, *N*-C*H*H-Ph), 6.47 (d, *J* = 15.6 Hz, 2H, *N*-CH*H*-Ph), 5.53 (d, *J* = 16.4 Hz, 2H, *N*-C*H*H-Py), 5.05 (d, *J* = 16.4 Hz, 2H, *N*-CH*H*-Py).^{13}C NMR (400 MHz, DMSO d_6) δ 170.32, 154.74, 153.15, 142.04, 141.29, 134.78, 134.05, 133.64, 133.54, 128.33, 127.59, 126.02, 125.06, 124.34, 124.15, 112.16, 111.52, 50.98, 50.54. $C_{40}H_{34}N_6NiBr_2{\cdot}C_4H_{10}O{\cdot}1.5H_2O$0.5 CH_3CN: Calcd. H 5.21, C 57.56, N 9.70; Found H 5.45, C 57.68, N 9.90. ESI-MS found (calculated): [M−2Br]$^{2+}$ *m*/*z* 328.1 (328.1).

4.6. [Ni(*L2*)$_2$]Br$_2$

H**L2**Cl (0.67 g, 2 mmol), anhydrous Ni(OAc)$_2$ (0.17 g, 1 mmol) and tetrabutylammonium bromide (1.5 g) were weighed into a 10 mL round-bottomed flask and dried for 4 h at 80 °C in a Schlenk setup under vacuum. The mixture was stirred for 48 h at 130 °C under vacuum, after which the mixture was let to cool and triturated with H_2O. The water layer was washed with DCM (3 × 20 mL), and a brown crystalline solid was obtained from the water solution in 5% yield (40 mg). ^{1}H NMR gave broad peaks. ^{13}C NMR spectrum was not recorded. ^{1}H NMR (300 MHz, DMSO-d_6) δ = 8.53, 8.32, 8.07, 7.57, 7.45, 7.41, 7.31, 7.08, 6.99, 6.43, 5.75, 4.96. MS *m*/*z* found (calc): [M−2Br]$^{2+}$ 329.1 (329.1). $C_{38}H_{32}N_8NiBr_2{\cdot}2.5H_2O$: Calcd. H 4.31, C 52.81, N 12.97; Found H 4.80, C 53.08, N 12.99.

Conflicts of interest

There are no conflicts to declare.

Acknowledgements

S. Luo gratefully acknowledges a grant from the Chinese Scholarship Council (no. 201306410011). We thank Dr. D.G.H. Hetterscheid for helpful discussions, and Mr. J.M.M van Brussel for ESI-MS measurements.

Appendix A. Supplementary data

Supplementary data associated with this article can be found, in the online version, at https://doi.org/10.1016/j.ica.2018.02.030.

References

[1] V.G. Organo, A.S. Filatov, J.S. Quartararo, Z.M. Friedman, E.V. Rybak-Akimova, Inorg. Chem. 48 (2009) 8456–8468.
[2] P. Zhang, M. Wang, Y. Yang, D. Zheng, K. Han, L. Sun, Chem. Commun. 50 (2014) 14153–14156.
[3] E.I. Musina, V.V. Khrizanforova, I.D. Strelnik, M.I. Valitov, Y.S. Spiridonova, D.B. Krivolapov, I.A. Litvinov, M.K. Kadirov, P. Lonnecke, E. Hey-Hawkins, Y.H. Budnikova, A.A. Karasik, O.G. Sinyashin, Chem. Eur. J. 20 (2014) 3169–3182.
[4] J. Berding, T.F. van Dijkman, M. Lutz, A.L. Spek, E. Bouwman, Dalton Trans. (2009) 6948–6955.
[5] R. Tatematsu, T. Inomata, T. Ozawa, H. Masuda, Angew. Chem. 55 (2016) 5247–5250.
[6] A. Kochem, M. O'Hagan, E.S. Wiedner, M. van Gastel, Chem. Eur. J. 21 (2015) 10338–10347.
[7] P.F. Huo, C. Uyeda, J.D. Goodpaster, J.C. Peters, T.F. Miller, ACS Catal. 6 (2016) 6114–6123.
[8] D.L. DuBois, R.M. Bullock, Eur. J. Inorg. Chem. (2011) 1017–1027.
[9] M.L. Helm, M.P. Stewart, R.M. Bullock, M.R. DuBois, D.L. DuBois, Science 333 (2011) 863–866.
[10] G.M. Jacobsen, J.Y. Yang, B. Twamley, A.D. Wilson, R.M. Bullock, M.R. DuBois, D. L. DuBois, Energy Environ Sci. 1 (2008) 167–174.
[11] P.D. Tran, J. Barber, Phys. Chem. Chem. Phys. 14 (2012) 13772–13784.
[12] D.J. Martin, B.D. McCarthy, C.L. Donley, J.L. Dempsey, Chem. Commun. 51 (2015) 5290–5293.
[13] N. Queyriaux, R.T. Jane, J. Massin, V. Artero, M. Chavarot-Kerlidou, Coord. Chem. Rev. 304–305 (2015) 3–19.
[14] J. Wang, C. Li, Q. Zhou, W. Wang, Y. Hou, B. Zhang, X. Wang, Catal. Sci. Technol. 6 (2016) 8482–8489.
[15] Q.-X. Liu, H.-L. Li, X.-J. Zhao, S.-S. Ge, M.-C. Shi, G. Shen, Y. Zang, X.-G. Wang, Inorg. Chim. Acta 376 (2011) 437–445.
[16] C. Chen, H. Qiu, W. Chen, J. Organomet. Chem. 696 (2012) 4166–4172.
[17] X. Zhang, S. Gu, Q. Xia, W. Chen, J. Organomet. Chem. 694 (2009) 2359–2367.

[18] L.B. Munro, V.J. Catalano, Eur. J. Inorg. Chem. (2014) 4994–5007.
[19] K. Chen, M.M. Nenzel, T.M. Brown, V.J. Catalano, Inorg. Chem. 54 (2015) 6900–6909.
[20] S. Das Adhikary, T. Samanta, G. Roymahapatra, F. Loiseau, D. Jouvenot, S. Giri, P. K. Chattaraj, J. Dinda, New J. Chem. 34 (2010) 1974–1980.
[21] J.-N. Luy, S.A. Hauser, A.B. Chaplin, R. Tonner, Organometallics 34 (2015) 5099–5112.
[22] J. Liu, M. Liu, Y. Yue, M. Yao, K. Zhuo, Chin. J. Chem. 30 (2012) 644–650.
[23] M.H. Reineke, M.D. Sampson, A.L. Rheingold, C.P. Kubiak, Inorg. Chem. 54 (2015) 3211–3217.
[24] L. Yang, D.R. Powell, R.P. Houser, Dalton Trans. (2007) 955–964.
[25] G. Armendariz-Vidales, C. Frontana, Phys. Chem. Chem. Phys. 17 (2015) 29299–29304.
[26] C. Costentin, J.-M. Saveant, ChemElectroChem 1 (2014) 1226–1236.
[27] M.T.M. Koper, E. Bouwman, Angew. Chem. Int. Ed. 49 (2010) 3723–3725.
[28] G.M. Sheldrick, Acta Crystallogr. Sect. A: Found. Crystallogr. 64 (2008) 112–122.
[29] G.M. Sheldrick, Acta Crystallogr. C Struct. Chem. 71 (2015) 3–8.
[30] J. Dinda, S.D. Adhikary, S.K. Seth, A. Mahapatra, New J. Chem. 37 (2013) 431–438.
[31] J. Berding, M. Lutz, A.L. Spek, E. Bouwman, Organometallics 28 (2009) 1845–1854.
[32] S. Luo, M.A. Siegler, E. Bouwman, Eur. J. Inorg. Chem. (2016) 4693–4700.
[33] H.V. Huynh, C. Holtgrewe, T. Pape, L.L. Koh, E. Hahn, Organometallics 25 (2006) 245–249.